Dynamically Estimating Saturation Flow Rate at Signalized Intersections: A Data-Driven Technique

Hossein Moradi[a]*, Sara Sasaninejad[a], Sabine Wittevrongel[a], Joris Walraevens[a]

[a]*SMACS Research Group, Department of Telecommunications and Information Processing, Ghent University, Ghent, Belgium*

Hossein.Moradi@ugent.be

+32456253477

Dynamically Estimating Saturation Flow Rate at Signalized Intersections: A Data-Driven Technique

Connected Vehicles (CVs) could enhance traffic management systems by providing detailed and real-time information. Theoretically, such information can be exploited for the provision of efficient movement of traffic, especially at intersections identified as the bottlenecks of traffic systems. Aimed at the same purpose, this paper uses the information of CVs to estimate the Saturation Flow Rate (SFR), particularly in the transition period during which CVs and conventional vehicles will coexist. To this end, we retain the advantages of data-driven techniques to capture the underlying dynamics of SFR by considering the information of CVs as the only input. In this regard, we correlate the dynamic variations of SFR to the mutual interactions among the contributing parameters extracted from the limited pieces of CVs' information using a neural network. Comprehensive simulations under precisely designed settings in VISSIM show a hoped-for SFR estimation accuracy level, which can further augment intelligent intersection controller initiatives.

Keywords: Dynamic saturation flow rate; Connected vehicles; Mixed traffic; Neural network; VISSIM

Introduction

With the soaring traffic congestion in urban areas, experts have been proposing traffic control methods to maximize the capacity of urban traffic networks. In this respect, by focusing on intersections as the critical bottlenecks of traffic and (particularly) using the information of Connected Vehicles (CVs)[1] as the new source of information, traffic control methods have been continuously improved (Guo, Li, et al. 2019; Moradi et al. 2022). However, despite the importance of the Saturation Flow Rate (SFR) in many of such emerging methods (see, for example, the models proposed in (He et al. 2014; Yang

[1] Connected vehicles are defined as vehicles that can communicate by any means.

et al. 2017; Moradi et al. 2021)), not much research has been done to enhance (accordingly) the quality[2] of SFR estimation models.

SFR determines the maximum flow rate (in a time unit) of a certain lane group if the associated traffic signal is constantly green (TRB 2010). In principle, SFR at a signalized intersection is a pivotal aspect of the capacity theory playing an important role in many efficiency indices, including delay and queue length. To date, three general approaches have dominated the methodologies applied to obtain SFR estimation models: (1) the adjustment approach, (2) the headway approach, and (3) the case-based approach.

Models developed using the adjustment approach (proposed in the U.S. Highway Capacity Manual HCM) and its variants are perhaps the most frequently proposed SFR estimation models over the past few decades due to their structural expressiveness[3]. Such models statically include coefficients to reflect the impact of site-specific parameters on a defined base SFR per lane, see (Lin 1992; Milazzo et al. 1998; Bonneson 2005; Potts et al. 2007; Shao et al. 2011; Chen et al. 2012; Guo et al. 2012; Chen et al. 2014; Behbahani et al. 2017; Biswas et al. 2018) for detailed information regarding the effects of these parameters on a base SFR. To obtain a better estimation of SFR in special cases, modifications have been further carried out (locally) to address the heterogeneous characteristics of infrastructures, vehicles, and drivers (e.g., the model presented in (Qin et al. 2019) considered the effects of guideline markings, (Anusha et al. 2013) focused on the high proportion of two-wheelers, and (Akçelik 2008) evaluated the effects of drivers'

[2] The term quality can be interpreted by (1) fitness for the intended purpose, (2) meeting the needed precision, and (3) satisfying simplicity and generalization issues.

[3] This concept refers to the power of a model's structure to incorporate contributing elements and to be interpreted as such element.

culture). Furthermore, these models have also been extended to capture the interaction effects among influencing parameters to improve the estimation accuracy of SFR (see (Wang, Rong, Zhou, Chang, et al. 2020) as an example).

The adjustment approach is based on static assignments that are well-suited for spatial constraints. While the spatial constraints of each specific intersection are, to a certain degree, responsible for SFR, the same intersection can have substantially different SFR values with respect to time-varying parameters resulting from dynamicity and stochasticity inherent in traffic (e.g., the current traffic composition, the flow pattern, the supply condition, and the temporal blockages, which all vary from time to time). To address this concern, several research studies have been conducted to estimate SFR by analyzing vehicles' real-time time-space information characterized by discharge headway values. For example, (Yang et al. 2013) and (Wang et al. 2018) proposed to use induction coil detectors and video detectors (respectively) as the data extraction tools to calculate the current discharge headway by applying an exponential smoothing method and the Dickey-Fuller test (respectively) to, eventually, approximate the current SFR. However, studies showed that models developed using the headway approach may result in an inaccurate estimation of SFR (Shao and Liu 2012), mainly due to the lack of expressiveness of this approach.[4]

Concerning the issue of accuracy, research projects on the development of SFR estimation models under the consideration of specific microscopic traffic conditions have also been ongoing. As a case in point, (Saha et al. 2018) proposed a model based on Kriging variants by using data collected from different cities in India. In another case, a regression model estimating SFR has been developed using data collected from

[4] In this case, we are restricted to a single variable equation derived from the average headway.

Bangladesh (Hossain 2001). Such models generally result in more accurate estimations of SFR than those from models developed by the adjustment or the headway approach. However, taking all microscopic factors into account renders such case-based models computationally intensive with a concomitant effect on their generalizability and applicability.

It can be seen from the above explanations that while previous models share a similar overall structure in terms of employing a set of data collected over a time period to estimate SFR, they differ from one another with respect to (1) how and in what detail they collect data and (2) in which way they estimate SFR using the collected data. Concerning the first difference, CVs are expected to have a high penetration rate in the near future, and are envisioned to provide much data in real-time for a low price (as opposed to traditional data collectors). Nevertheless, a limited effort to build SFR estimation models using the information of CVs has, to the best of the authors' knowledge, been reported in literature. Concerning the second difference, it appears from literature that not much research has been done to develop a model combining (1) expressiveness from the adjustment approach, (2) dynamicity from the headway approach, and (3) accuracy from the case-based approach.

Given these research gaps, this study contributes to the literature by proposing a CV-based neural network model (which, from now on, we will refer to as *CVN-SFR*) to dynamically estimate the SFR of each lane by relying on CVs as the only source of information. In this case, note that there are studies using information of CVs to construct the fundamental diagram, see (Guo, Xiao, et al. 2019; Seo et al. 2019; Guo and Zhang 2021). Such models can be used to macroscopically determine the maximum traffic flow without incorporating heterogeneity in the traffic composition, driving behaviors, or temporary obstacles (e.g., bus stops and pedestrians), to name only a few examples.

However, we aim to look at this issue microscopically to address the effects of temporal characteristics of traffic on SFR. In this respect, it should be pointed out that while previously proposed models could relate changes in SFR to spatial and site-specific parameters, the relationship between SFR and information of vehicles, in general, and CVs, in particular, is poorly understood. Accordingly, given the confirmed advantages of neural network models in handling different types of interactions when underlying dynamics are unknown (Karlaftis and Vlahogianni 2011), we employ neural network models to estimate SFR. Under this approach, first, we can leverage the expressiveness of *CVN-SFR* by using a network structure that consists of several hidden layers along with activation functions. Second, the resulting model, which is purely data-driven, can address the required dynamicity through the analysis of real-time information of CVs. Third, given a better understanding of underlying dynamics, *CVN-SFR* is expected to act in pursuit of maximizing the accuracy of SFR estimations.

It is important to note that while CVs will become more prevalent in the near future, they will certainly coexist with conventional vehicles for an enduring time horizon due to the general characteristics of technology diffusion. Given this point and also considering that deploying traffic sensors (e.g., detectors) everywhere is neither cheap nor easy, it is particularly not a promising approach (at least in the near future) to look at such issues from a fully connected environment standpoint. Hence, *CVN-SFR* is developed under the assumption of incomplete and sparse data resulting from mixed traffic conditions (consisting of both CVs and conventional vehicles). To simulate this condition as realistically as possible, we use the microscopic simulator VISSIM as the data generating tool in this study due to its comparative advantages in modeling multiple types of vehicles in different road network configurations managed by distinct methods.

Based on the resulting data, we further use our model in a plethora of experiments to evaluate the accuracy of its estimations.

The remainder of this paper is structured as follows. Section 2 defines the simulation settings used in the data generation processes. Section 3 focuses on the data collection processes and reveals the rationale behind the chosen parameters. Section 4 explains the structure of our model and illustrates the core functionality of *CVN-SFR*. Finally, Section 5 enumerates the main conclusions.

Simulation settings

As mentioned, VISSIM is adopted here to generate traffic data comparable to what one may observe in real-world situations. This section details how this microscopic simulator has been prepared for this purpose by defining different types of intersections, which are dynamically loaded with widely differing traffic fleets.

Defining intersections

Defining all kinds of geometries and configurations for an intersection without resorting to any specific structure is difficult to achieve, if not impossible. However, simulating a general intersection structure under different assumptions can be regarded as a solution giving rise to the observation of many possible real-world situations. Accordingly, we define a typical four-leg intersection configuration as our base case to which different scenarios in terms of

- the number of lanes in each leg,
- speed limits with respect to different area types,
- whether or not there are any parking slots, bus stops, walking (and bicycle)

signals, or zebra lines,

- signal controller mechanisms

are applied.

In light of the latter, it should be mentioned that the drive to include different mechanisms for signal sequences in an intersection arises from the identified effect of internal conflict points on the value of SFR. To have an intuitive sense of this issue, we borrow the simple example provided by (Flötteröd and Rohde 2011) as is depicted in Figure 1. In this three-leg intersection (where each leg has one lane), the applied intersection control method simultaneously gives the right-of-way (green light) to the north flow with a right-turning share and the south flow with a left-turning share. We assume that the capacity of the westbound link is fully used by the left-turning share of the south flow demand and the right-turning share of the north flow demand (i.e., queues of vehicles have been formed in the south and north legs). Accordingly, we can infer that if in *conflict point A* the north flow demand yields to the south flow demand (based on the priority rules and also differences with respect to the drivers' compliance to those rules), the larger share of the south flow demand will cross the intersection.

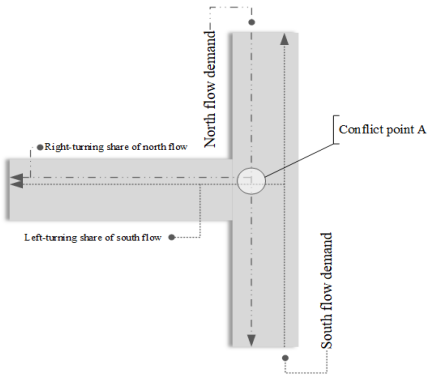

Figure 1. A single-lane three-leg intersection where SFR is affected by internal conflicts.

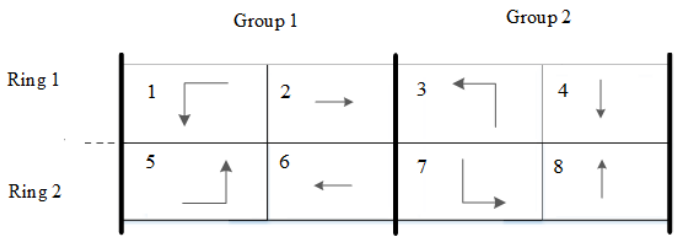

Figure 2. The standard NEMA structure.

Generally, given that different conflict points could appear under different mechanisms for signal sequences in an intersection, we define distinct types of intersections with respect to their control methods. To do so, we consider different sequences of the possible signal groups categorized using the standard NEMA (National Electrical Manufacturers Association) dual-ring structure shown in Figure 2. Based on this structure, straight and left-turning signal movements (which are labeled by even and odd numbers, respectively) form two groups, each of which consists of two rings. Using these groups and rings, the compatible signal groups can be identified (e.g., signal movements 1 and 6) and determined for the phase allocations (with and without permitted right-turning movements).

Defining traffic fleets

Characterization of traffic fleets is carried out here by (1) defining different types of vehicles, (2) designing multiple patterns of individual driving behavior, and (3) considering different mixes of vehicles controlled by different drivers.

First, different types of vehicles are supplemented to the model. To do so, we define Heavy Goods Vehicles (HGVs), buses, passenger vehicles, motorcycles, and bicycles by considering different specifications in terms of *maximum speed*, *maximum acceleration*, *maximum deceleration*, and *occupancy area*. We also assume that the

effects of site-specific conditions of a given intersection (e.g., grade, weather, visibility, etc.) on the operation of vehicles have previously been reflected in the provided specifications. Moreover, to deal with the communication capability of CVs, we define and enable a Boolean attribute to discriminate between CVs and conventional vehicles in terms of the ability to send information.

Second, we define different sets of driving behavior, including conservative, normal, and aggressive (turn-taking) models, to address the heterogeneity of drivers in terms of respecting the priority rules. To this end, we adjust the parameters of the car-following, lane-changing, and lateral behavior settings available in VISSIM using defined ranges given in (AG 2018) to derive different behavior models. Then, every vehicle is randomly subjected to one of these driving behavior models to satisfactorily represent real-world observations in which each driver responds differently and unpredictably to the same stimuli.

Third, we define the scenarios illustrated in Figure 3 to define different mixes of traffic fleets. Specifically, we separately consider *scenario* 1: a low proportion of two-wheelers (i.e., both motorcycles and bicycles) and heavy vehicles (i.e., both HGVs and buses), *scenario* 2: an average proportion of heavy vehicles, *scenario* 3: a high proportion of heavy vehicles, *scenario* 4: a high proportion of HGVs, *scenario* 5: a high proportion of buses, *scenario* 6: an average proportion of two-wheelers, *scenario* 7: a high proportion of two-wheelers, *scenario* 8: a high proportion of motorcycles, and *scenario* 9: a high proportion of bicycles. For the sake of illustration in the above scenarios, we assume the 2%, 12%, and 22% (respectively) proportion of each specific type of vehicles to represent the low, average, and high proportion (respectively) of that type of vehicles in traffic.

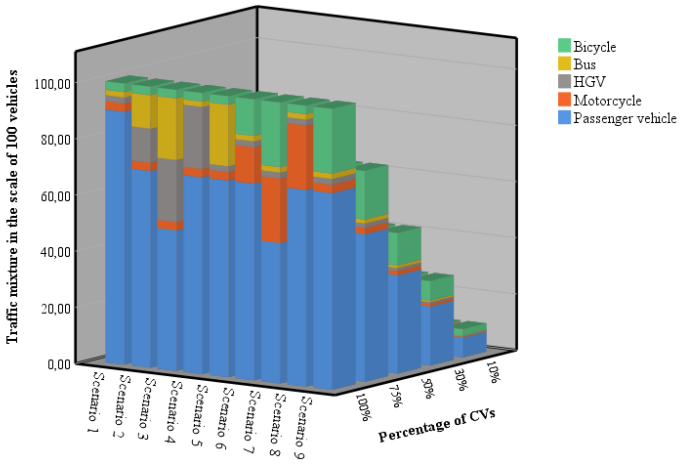

Figure 3. Different traffic fleet mixes configured for this study.

Simulation and data generation

For generating data, we first activate the dynamic traffic assignment option during the simulation in VISSIM, as this is expected to result in a more realistic distribution of traffic demand and supply. Then, by iteratively changing the arrival rates of different traffic fleets in each specific intersection, we simulate the flow of traffic and generate traffic data.

Data collection

This section is dedicated to reviewing the data collection processes of parameters (selected to train the model) in both the input and the output layers of the neural network.

Data quality attributes

The reliability of data-driven techniques, in general, and neural network models, in particular, tremendously depends on the amount and quality of the collected data. In other words, the performance of such models will significantly deteriorate if the collected data suffers from inaccuracy, scarcity, inconsistency, or irrelevancy.

In reality, there is still a long way remaining to achieve such a goal of whole traffic data extraction through a number of CVs equipped with different kinds of sensors capable

of onboard data analysis. However, considering the increasing progress in the technology of CVs (Uhlemann 2015), it is not fictional to assume that CVs can transmit their own information to an information unit (i.e., V2I) accurately without failure. Accordingly, considering the effect of data inaccuracy may not be essential in this work.

The issue of data scarcity, on the contrary, directly depends on the proportion of CVs in a traffic composition, as it is assumed here that only CVs can report data. As is shown in Figure 3, different percentages of CVs in various traffic compositions are used to ensure the robustness of the model in case of sparse data. To overcome data scarcity in case of a low proportion of CVs, we can (1) adopt approaches revealing the correlations among different pieces of CVs' data (e.g., correlation matrices (Gao et al. 2017) or principal component analysis (Abdi and Williams 2010)), or (2) embed auxiliary parameters to relate between estimations of *CVN-SFR* in different lanes and different cycles. The latter is selected here to be implemented due to its computational convenience.

The issue of data inconsistency could become a major concern, especially after the commercialization of CVs by different companies at an affordable price. In that case, various sets of data notation and terminology utilized by different companies induce non-homogeneities in datasets. Accordingly, to retain consistency among data residing in datasets, emerging data storing techniques should eventually be employed in data collection processes.[5] However, we assume here that all pieces of data are consistent.

[5] A rigorous analysis of the transformation of CVs' data into a suitable form for data mining purposes is left for future research.

Finally, concerning the issue of data irrelevancy, we choose to conduct focus group discussions (Hennink 2013) aiming at finding the most relevant CVs' data in the context of SFR and ignore further details. The importance of this step is in the fact that pulling information from massive data is too expensive in terms of processing time, not to mention the required technological capacity that is lacking in many cases. According to the carried out sessions, among the available pieces of CVs' data in a time horizon with predetermined cycle durations, the followings are believed to have great promise and be practically accessible:

(1) N_i^k : total number of CVs in lane i during cycle k (where a cycle starts just after the beginning of the corresponding red time and ends before the signal turns red again). For example, see points 1 to 5 in Figure 4 ($N_i^k = 5$).

(2) B_i^k : total number of stop-and-go events of CVs in lane i during cycle k. Points 6, 7, and 8 in Figure 4 highlight such events.

(3) P_{ik} : total number of CVs in lane i at the end of cycle k. As an example, given points 9 and 10 in Figure 4, P_{ik} for this case is equal to 2.

(4) D_{ik}^p : distance of CV p to the signal head of lane i at the end of cycle k. Such variables are shown by arrows with numbers 11 and 12 in Figure 4.

(5) V_{ik}^p : speed of CV p in lane i at the end of cycle k. This information can be derived from the trajectory information of each CV, as is shown by points 13 and 14 in Figure 4.

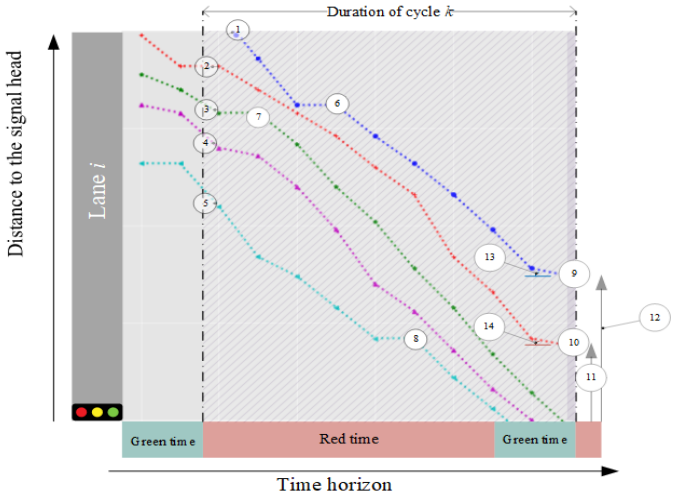

Figure 4. A time-space diagram of the trajectories of CVs at lane i during cycle k.

Input layer: the information of CVs

In the ongoing effort to estimate SFR, we need to reformat the available pieces of CVs' data in such a way that they represent the mutual interaction between the time-invariant intersection parameters and the varying characteristics of traffic flows. To this end, we propose the input parameters as are enumerated below (from A_1 to A_5):

(1) $A_1 = \dfrac{N_i^k}{\sum_{i \in I} N_i^k}$;

A_1 is the number of CVs approaching the intersection through lane i during cycle k divided by the total number of CVs approaching the intersection (considering the set of all lanes I) during that cycle. As A_1 gets values closer to *1* (*0*), it means that the relative demand in lane i is higher (lower), compared to other lanes. Moreover, a value close to $1/n(I)$ (where the notation n(*I*) indicates the number of elements in the set *I*) for A_1 implies that the current traffic demand is uniformly distributed among all lanes. Accordingly, this parameter is deemed to be related to the temporal characteristics of traffic in terms of the arrival pattern. Note that

arrival patterns could affect the way congestion grows in space and time.

(2) $A_2 = \frac{B_i^k}{N_i^k} / \sum_{i \in I} \frac{B_i^k}{N_i^k}$;

A_2 is the average number of stop-and-go events (per CV) in lane i during cycle k as compared to the average number of stop-and-go events in all lanes in that cycle. This parameter is expected to, on the one hand, be related to the effects of bus stops, parking slots, and zebra lines, and on the other hand, reflect the internal constraints (originating from an intersection control method) or supply blockages. In fact, in a certain demand profile, there are generally more stops if traffic demand is subjected to (1) extra moving bottlenecks (e.g., bus stops, pedestrians, etc.) or (2) intersection internal and supply constraints, which both could considerably change SFR.

(3) $A_3 = \sum_{p=1}^{P_{ik}} (\frac{V_{ik}^p}{V_{all_i}^p} \cdot \frac{1}{D_{ik}^p}) / P_{ik}$;

A_3 is the average of the product of each CV's normalized speed in lane i at the end of cycle k with the inverse of its scaled associated distance to the signal head.[6] Considering the Greenshields fundamental relations (Kessels 2019), this parameter gives an implicit exhibition of flow and congestion in lane i, while also putting more weight on the speed of CVs closer to the intersection. Accordingly, in relation with other indicators describing congestion (e.g., A_1 and A_2), A_3 can lead to the representation of the current traffic behavior at lane i in terms of flow.

[6] Normalized speed refers to CVs' speed in lane i divided by the allowable speed of CV p in lane i (labeled by $V_{all_i}^p$).

(4) $A_4 = \sqrt{\frac{1}{P_{ik}-1}\cdot\sum_{p=1}^{P_{ik}}(\frac{V_{ik}^p}{V_{all_i}^p}-\frac{1}{P_{ik}}\cdot\sum_{p=1}^{P_{ik}}\frac{V_{ik}^p}{V_{all_i}^p})^2}\,/\,(\frac{1}{P_{ik}}\cdot\sum_{p=1}^{P_{ik}}\frac{V_{ik}^p}{V_{all_i}^p})$;

A_4 is the standard deviation of the CVs' normalized speed in lane i at the end of cycle k multiplied by the inverse of the average of the normalized speed in lane i at the end of cycle k.[7] This is a formulation that is used to calculate the *coefficient of variation* measuring the dispersion of speed distribution. This parameter is used to deal with the heterogeneity of road users with respect to their operating differences. To better explicate the implications of this parameter, recall that we define different types of vehicles with different specifications, including *speed*. Accordingly, under a heterogeneous traffic fleet, there could be some temporary blocking events (meaning some vehicles cannot go towards an intersection with the desired speed) which will be highlighted by this parameter.

(5) $A_5 = \frac{\|[S_{i'}^k \mid \forall i' \rightarrow i' \neq i \wedge N_{i'}^k \neq 0 \wedge P_{i'k} \neq 0]\|_1}{\|[S_{i'}^k \mid \forall i' \rightarrow i' \neq i \wedge N_{i'}^k \neq 0 \wedge P_{i'k} \neq 0]\|_2}\cdot\frac{S_i^{k-1}}{\sum_{i\in I}S_i^{k-1}}$;

A_5 is the ratio of the first norm of the vector consisting of all other SFR values except i (labeled by $S_{i'}^k$) to its second norm, multiplied by the ratio of S_i^{k-1} to the sum of all SFR values at cycle $k-1$. We have defined A_5 to relate between SFR of lane i at cycle k with (1) SFR of other lanes in cycle k and (2) SFR of lane i at cycle $k-1$ to contribute in the case of a low proportion of CVs. The defined parameter can make the connection with the SFRs of other lanes during the current cycle and with the SFR of the previous cycle.

[7] To calculate the standard deviation, we assume our available data as a sample space.

Output layer: the SFR results

To calculate S_i^k, many studies have used the concept of *passenger car unit* (Raj et al. 2019) to deal with the issue of headway differences between different types of vehicles (see (Chand et al. 2017)). Despite the incurred complexity of this concept (Arasan and Arkatkar 2008), however, (Radhakrishnan and Mathew 2011) has found that using *passenger car unit* in a highly heterogeneous traffic flow might lead to an erroneous outcome. Accordingly, we alternatively use

$$S_i^k = \frac{TN_i^{g_e^k}}{g_e^k} \cdot 3600 \tag{1}$$

which calculates S_i^k in terms of *(vehs/lane)/h* by considering the count of all vehicles $TN_i^{g_e^k}$ in lane i crossing the stop line of the intersection during the associated effective green time at cycle k (labeled by g_e^k and measured in seconds) (Saha et al. 2018). By doing so, we also incorporate the effect of lane width on SFR, which is especially important when the proportion of two-wheelers is relatively high.

It should also be mentioned that in Equation (1), g_e^k refers to a time during which traffic may proceed at SFR. Theoretically, g_e^k starts after the start-up lost time (mainly occurring due to the shockwave phenomenon (Michalopoulos and Stephanopoulos 1981)) and lasts until the green time duration ends or there are fewer number of vehicles than a predefined threshold[8] to discharge, whichever comes first (Tan et al. 2013). A schematic representation of g_e^k and $TN_i^{g_e^k}$ is provided in Figure 5.

[8] We assume a minimum of 5 vehicles as this threshold.

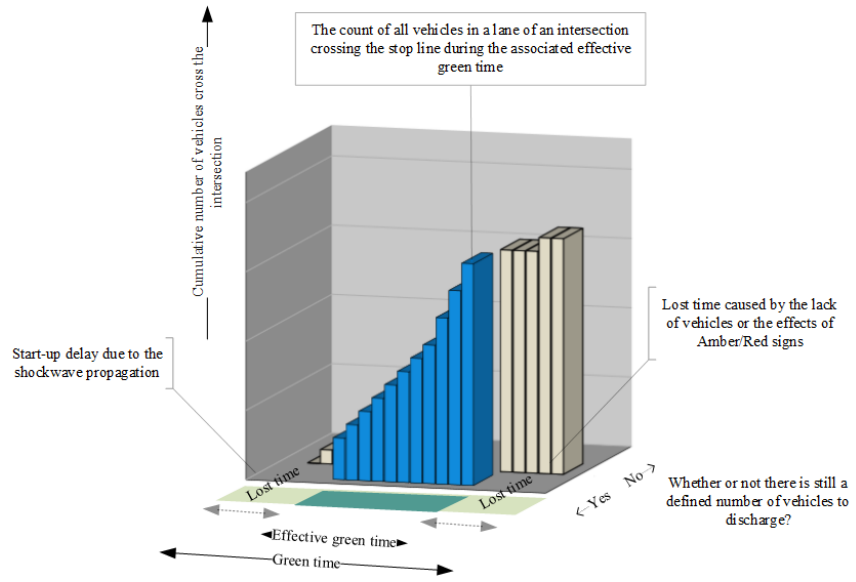

Figure 5. An illustration of the effective green time and the count of vehicles crossing the intersection during this time.

Model development and evaluation

This section first demonstrates how *CVN-SFR* is built, then evaluates its functionality, and finally clarifies its potential implications in the context of intersection and traffic management.

Architecture of CVN-SFR

Figure 6 represents a conceptual illustration of *CVN-SFR*. As is shown in this figure, the apparatus of *CVN-SFR* consists of three processes: (a) extracting the input parameters based on CVs' data at each cycle, (b) feeding these parameters into a defined neural network, and (c) checking whether or not the estimated SFR meets the accuracy requirement. Note that we have already explained the parameter extraction process (see Figure 6 (a)) in the previous section. The current section thus continues to provide insight into the latter two processes.

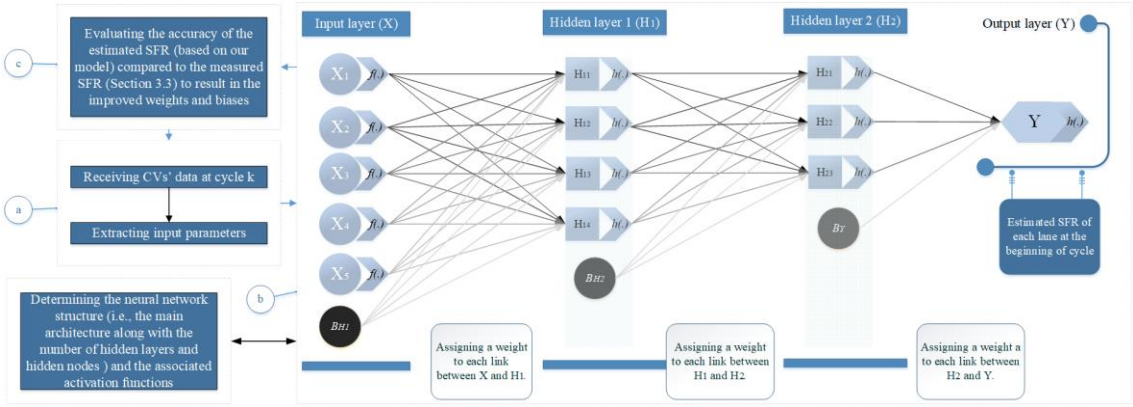

Figure 6. A conceptual representation of CVN-SFR.

To define a neural network, we should first determine its *neurons* (also called *nodes*) characteristics. A neuron is the basic building block that takes an arbitrary number of input signals, performs a mathematical operation to each input, and results in an output signal. As is customary in the related literature, previously proposed activation functions (such as the sigmoid, hyperbolic tangent, and rectified linear unit functions (Lau and Lim 2017)) can be employed in neurons as the mathematical operator to nurture the imitation capability. Among these functions, we select the sigmoid function (i.e., $f(a)=1/1+e^{-a}$ for any input, say a) and the rectified linear unit (i.e., $h(b)=\max(0,b)$ for any input, say b). The drive to embed these functions in our model arises from the need to (1) ensure bounds on each input signal and (2) allow for positive SFRs only. Furthermore, we have also inserted bias units (B_{H_1}, B_{H_2}, and B_Y in Figure 6 (b) for neurons in the H_1, H_2, and Y layers, respectively) into our model to add new dimensions in the computation processes with the capability of shifting the activation functions.

Arranging the defined neurons and biases (whose possible magnitudes will be obtained from the learning algorithm) in series and parallel (and even both) along with considering links (whose weights will also be generated by the adopted learning algorithm) to connect neurons (with respect to their weights) will provide the ability of pattern recognition in a network as a whole. Accordingly, the vast set of neural network

architectures have been presented so far by defining different ways in which neurons are interrelated (e.g., feed-forward, recurrent, and convolutional neural networks, to name only a few (Brunton and Kutz 2022)). Among them, we adopt the feed-forward structure along with the assumption of a dense connection between the defined neurons to solve for the estimation of current SFR due to its reported power to deal with such prediction problems (Wang, Rong, Zhou, and Gao 2020).

Working within a densely connected feed-forward network structure, we should now identify the necessary number of hidden layers and also the number of neurons in each hidden layer (i.e., the regularization of hyper-parameters). Determination of these parameters is not a straightforward task since it not only depends on the intended structure and the number of input and output units but also entails an analysis of the training samples and the training algorithm (e.g., *K-fold cross validation*) (Ke and Liu 2008). However, it has been proved that for many tasks (including such non-linear approximations), using shallow networks (consisting of one or two hidden layers) can give satisfactory predictions with sufficiently small error (Cai et al. 2019). Accordingly, by opting for a network with two hidden layers, we can use approximation methods previously proposed to estimate the appropriate number of hidden neurons (Gentile and Sznaier 2001; Vasilyev 2016). In particular, the authors of (Vasilyev 2016) used the minimal complexity principle to present (see Figure 6)

$$n(H_2) \geq \left\lceil \frac{n(Y)\cdot(R-n(H_1))}{n(X)+n(H_1)} \right\rceil \tag{2}$$

as a condition approximating the required number of hidden neurons in *hidden layer 1* $n(H_1)$ and hidden layer 2 $n(H_2)$, with respect to the number of input parameters $n(X)$, the number of output parameters $n(Y)$, and the number of prevalent modes R. To

determine the number of prevalent modes, recall that we define four input parameters[9] (i.e., A_1 to A_4) representing the different modes leading to the determination of SFR. This means that in each distinct mode, there is a specific arrangement of these parameters ordered according to their influence on SFR. Hence, by considering $R = 4$, $n(X) = 5$, and $n(Y) = 1$, we see that the condition presented in Equation (2) will be met by having four neurons in *hidden layer 1* (i.e., $n(H_1) = 4$) and three neurons in *hidden layer 2* (i.e., $n(H_2) = 3$). All this taken into account, we use a network structure shown in Figure 6 (b) resulting in a total of 43 weights and biases to be optimized.[10]

To this end, by reviewing the literature of neural networks with prediction purposes (Adya and Collopy 1998), we found that the widely used backpropagation algorithm (Hecht-Nielsen 1992) could be effectively applied as the learning algorithm in our network (Figure 6 (c)). In this algorithm, the computation starts with considering a random weight for each link (e.g., $W_{H_1}^{X}(a,b)$ between neuron a in the input layer and neuron b in *hidden layer 1* and also assigning random biases (e.g., B_{H_1} inserted into *hidden layer 1*). Then, by selecting *mean squared error* as our loss function and *gradient descent* as the optimizer, this algorithm uses

[9] Note that A_5 is presented as an auxiliary parameter to boost the model's robustness.

[10] By using these approximations, we circumvent the need for a complex cross-validation for regularization.

$$\begin{cases} \Delta W_Y^{H_2}(c,d) = \alpha \cdot (S_i^k - h(d)) \cdot h'(d) \cdot h(c) \\ \Delta W_{H_2}^{H_1}(b,c) = \alpha \cdot (S_i^k - h(d)) \cdot h'(d) \cdot \sum_{c \in H_2} (W_Y^{H_2}(c,d) \cdot h'(c)) \cdot h(b) \\ \Delta W_{H_1}^{X}(a,b) = \alpha \cdot (S_i^k - h(d)) \cdot h'(d) \cdot \sum_{c \in H_2} [(W_Y^{H_2}(c,d) \cdot h'(c)) \cdot \sum_{b \in H_1} (W_{H_2}^{H_1}(b,c) \cdot h'(b))] \cdot f(a) \\ \Delta B_Y = \alpha \cdot (S_i^k - h(d)) \cdot h'(d) \cdot h(c) \\ \Delta B_{H_2} = \alpha \cdot (S_i^k - h(d)) \cdot h'(d) \cdot \sum_{c \in H_2} (W_Y^{H_2}(c,d) \cdot h'(c)) \\ \Delta B_{H_1} = \alpha \cdot (S_i^k - h(d)) \cdot h'(d) \cdot \sum_{c \in H_2} [(W_Y^{H_2}(c,d) \cdot h'(c)) \cdot \sum_{b \in H_1} (W_{H_2}^{H_1}(b,c) \cdot h'(b))] \end{cases} \quad (3)$$

in each epoch to improve weights and biases (with respect to the previous iteration), in such a way that the minimum of the loss function can eventually be found. It should be mentioned here that in Equation (3), *d*, *c*, *b*, and *a* indicate node values in the output, *hidden layer 2*, *hidden layer 1*, and input layers, respectively. Given *a* (input), we further calculate these values by

$$\begin{cases} d = \sum_{c \in H_2} (W_Y^{H_2}(c,d) \cdot h(c)) \\ c = \sum_{b \in H_1} (W_{H_2}^{H_1}(b,c) \cdot h(b)) \\ b = \sum_{a \in X} (W_{H_1}^{X}(a,b) \cdot f(a)) \end{cases} \quad (4)$$

Furthermore, α (in Equation (3)) stands for the learning rate. The learning rate specifies how much each weight and bias can change with reference to the observed error (Thota and Changalasetty 2013). In this regard, on the one hand, caution should be taken to use large learning rates, which may inhibit the minimization of the loss function at any one time, and on the other hand, it should be considered that very small learning rates can

incur computational burden. In our model, $\alpha = 0.01$ turned out to be an appropriate learning rate according to the analysis of obtained loss values.[11]

Results of CVN-SFR

After adjusting the simulation settings based on the provided explanations, internal scripts[12] (coded in COM interface) are used to run the simulation operation and data collection processes. Subsequently, several sequences of 9-hour simulations have been performed in a way that:

- in each sequence of simulation, we combine a distinct intersection with a different proportion of CVs;
- in each hour of a simulation run, we use a different traffic fleet.

Prior to moving towards training and analyzing our model, there is a need to split collected data into training, validation, and test sets in order to (1) fit *CVN-SFR* through the use of the training set, (2) fairly assess the quality of *CVN-SFR* through the use of the validation set, and (3) evaluate the accuracy of the estimations of *CVN-SFR* in unprecedented (new) conditions through the use of the test set. Note that while both the validation set and the test set are not incorporated in the learning process, the validation set is obtained from similar experiments to that of the learning set, but on the other hand, the test set is obtained from different experiments in terms of intersections geometry and traffic fleets. Additionally, we aim to explore the effect of the penetration rate of CVs on

[11] The issue of computation speed is beyond the scope of this investigation. However, the interested readers can refer to (Andayani et al. 2017) for a method of accelerating a backpropagation algorithm.

[12] The scripts are available at https://github.com/HossseinMoradi/Project10

the accuracy of *CVN-SFR* estimations. The quantification of this matter is carried out by defining two test cases resulting in: *Test set 1* where all vehicles are connected and *Test set 2* in which the proportion of CVs is 10%. Figure 7 depicts a summary of the key attributes for each set.

Given these sets, to deal with missing data (emerging due to the simulation of mixed traffic), we adopt the imputation technique (Little and Rubin 2019). The main principle of all variants of this technique is to replace missing data with other (but relevant) values, to make the whole data set exploitable as if it was complete. In our case, we use the defined auxiliary parameter (A_5) as a *similarity score* to improve the quality of values resulting from imputation with the mean approach. In this regard, while imputation with the mean approach (by itself) is efficient and valid for our data set (due to its perceivable analogy to a normal distribution) (Brown and Kros 2003), we have further applied a simple algorithm with which the stationary results of the mean approach are adjusted with respect to the relative value of the corresponding similarity score. Using these completed sets, our analysis yields the following results.

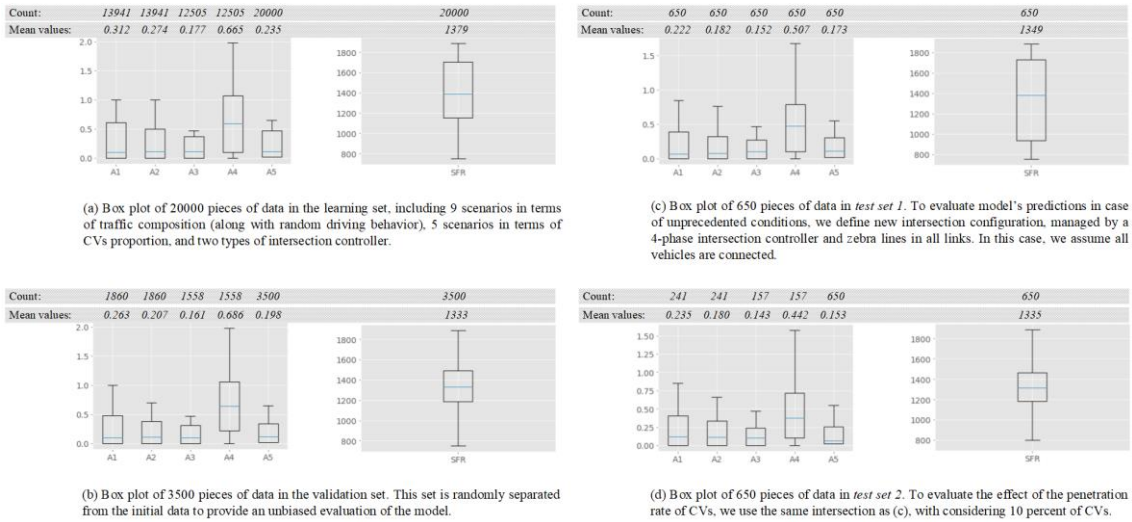

(a) Box plot of 20000 pieces of data in the learning set, including 9 scenarios in terms of traffic composition (along with random driving behavior), 5 scenarios in terms of CVs proportion, and two types of intersection controller.

(c) Box plot of 650 pieces of data in *test set 1*. To evaluate model's predictions in case of unprecedented conditions, we define new intersection configuration, managed by a 4-phase intersection controller and zebra lines in all links. In this case, we assume all vehicles are connected.

(b) Box plot of 3500 pieces of data in the validation set. This set is randomly separated from the initial data to provide an unbiased evaluation of the model.

(d) Box plot of 650 pieces of data in *test set 2*. To evaluate the effect of the penetration rate of CVs, we use the same intersection as (c), with considering 10 percent of CVs.

Figure 7. Classification of data sets.

With respect to the learning process, Figure 8 (a) shows how the value of the loss function changes over epochs. According to this figure, the obtained loss value incrementally decreases until the minimum loss value has been met. At this time, the learning process has been completed, and the values of weights and biases have converged. Performing qualitative reasoning on Figure 8 (a) can bring up the following arguments:

- According to the trajectory of the loss value, we can claim that the backpropagation algorithm equipped with the gradient descent optimizer and the defined learning rate has operated successfully.
- According to the resulted minimum loss value, we can conclude that the developed network structure is able to satisfactorily relate the defined input parameters and SFR.

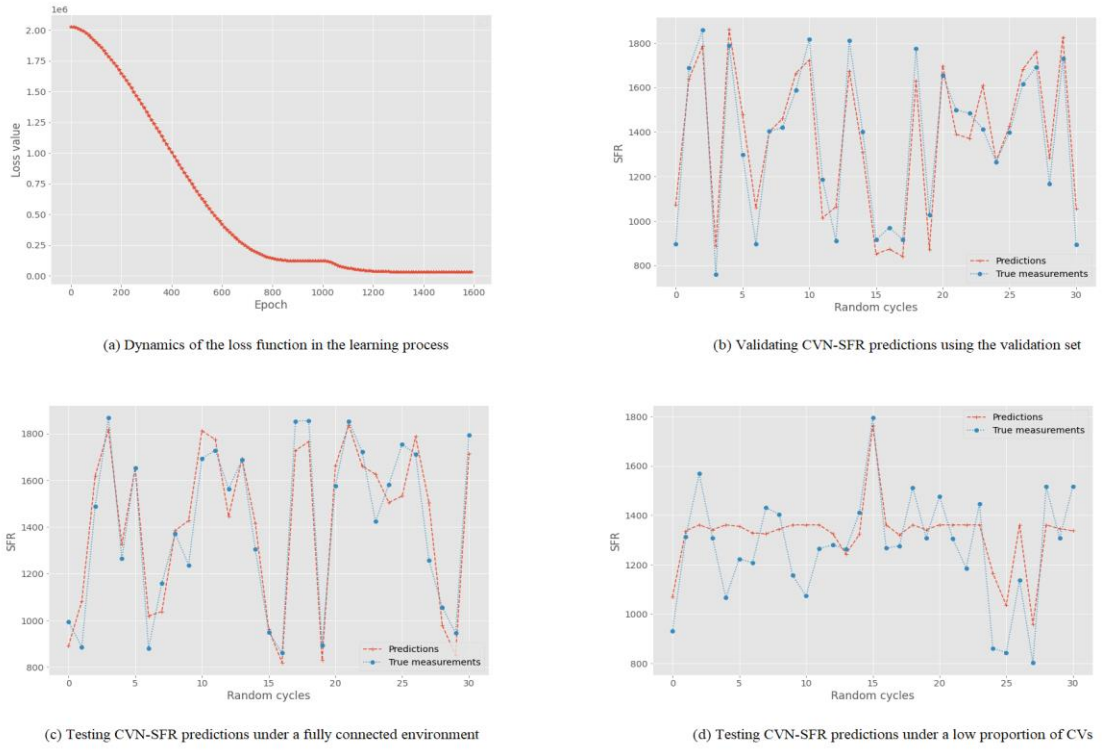

(a) Dynamics of the loss function in the learning process

(b) Validating CVN-SFR predictions using the validation set

(c) Testing CVN-SFR predictions under a fully connected environment

(d) Testing CVN-SFR predictions under a low proportion of CVs

Figure 8. Results of learning, validating, and testing processes of *CVN-SFR*.

With respect to the validation process, Figure 8 (b) highlights how accurate the trained model is in relation to the validation data set. Concerning this, we randomly selected data from the defined validation set and compared the predictions of *CVN-SFR* to the true SFR measurements. Carrying out this comparison, as is shown in Figure 8 (b), leads to the following arguments:

- When the validation set and training set are drawn from the same population, the (unbiased) results of *CVN-SFR* are, to a large extent, close to the true values;
- The set of input parameters proposed in this research can capture the dynamics of SFR under different intersection configurations and traffic fleet mixes.

Furthermore, we have also compared all SFR measurements in the validation set with the associated predictions of *CVN-SFR*. This comparison shows that the average error of *CVN-SFR* in this set is 10.7% and $R^2 = 0.81$. In other words, we see that the accuracy of *CVN-SFR* is around 90% for the validation set, and also the input parameters can considerably show the dynamic change of SFR, which in turn confirm the above-mentioned arguments, respectively.

With respect to the test process, Figure 8 (c) and (d) are provided to reveal the accuracy of *CVN-SFR* when it is exposed to unprecedented conditions. In this regard, Figure 8 (c) and (d) are respectively dedicated to two extreme cases in our simulation scenarios, namely (1) the percentage of CVs in the traffic fleet is 100% and (2) the percentage of CVs in the traffic fleet is 10%. The obtained results are interpreted as supporting the following arguments:

- In the case of fully connected traffic, the predictions of *CVN-SFR* are appropriately close to the true SFRs. Hence, our proposed model is able to predict SFR (per lane) based on the information of CVs in the intersection, without knowing the geometric properties of the intersection, the composition of the

traffic fleet, and the behavioral patterns of drivers. It is worth mentioning here that besides these random cycles, comparing all the *CVN-SFR* predictions with the corresponding SFR measurements in this set results in 15.3% as the average error, which, by considering the standard deviation of SFR measurements (see Figure 7), can be considered as a significant improvement;

- When the proportion of CVs is relatively low (10% in our case), the application of *CVN-SFR* leads to predictions with lower fidelity (i.e., by analyzing all cases, the average error is 27.4%). However, while the average of SFR predictions is still close to the average of SFR measurements, *CVN-SFR* has also captured the trend of SFR dynamics to an extent, something that conventional methods cannot do. Accordingly, even with a low proportion of CVs, *CVN-SFR* can outperform conventional SFR prediction models.

To shed more light on the latter, we analyze Figure 8 (d) from another perspective, as is shown in Figure 9. In an ideal case, what conventional models would predict (by considering the geometric properties of the intersection, the general composition of the traffic fleet, and the behavioral patterns of drivers) equals the average SFR (i.e., 1335) shown in Figure 9. Note that while many of SFR measurements fall within a range around this average value, it is possible to observe a relatively much higher (e.g., point 1) or lower (e.g., point 2) SFR (in Figure 9), due to the effect of time-varying traffic parameters like approaching a high number of two-wheelers, on the one hand, or pedestrian obstructions, on the other. In this case, we see that while the average of the estimated SFRs (i.e., 1365) is close to that of true values, significant changes of SFR have also been captured by *CVN-SFR* to some degree (see predictions at points 1 and 2). Such comprehensions enable *CVN-SFR* to perform better than conventional SFR prediction models even with a low proportion of CVs.

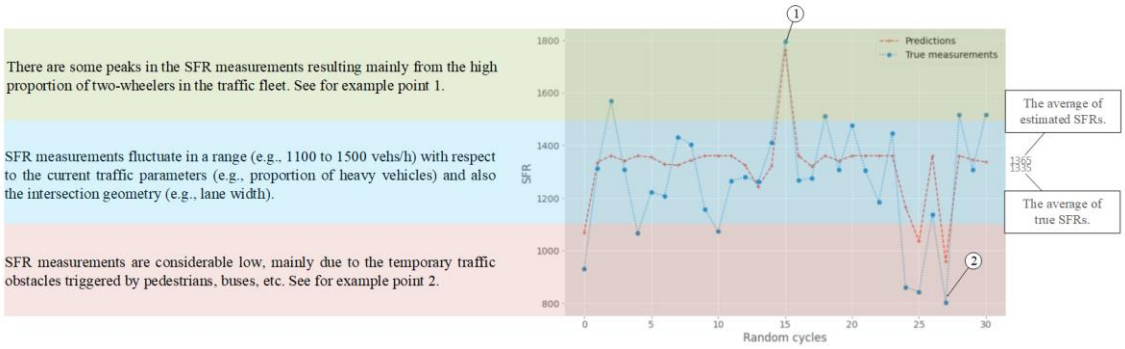

Figure 9. The estimations of *CVN-SFR* under a low proportion of CVs.

Finally, we carry out a sensitivity analysis to assess the influence of each input parameter on the predictions of *CVN-SFR*. In this regard, we train our model four more times, in each of which we have eliminated one of the defined input parameters (A_1 to A_4) and, then, have used the same network structure as *CVN-SFR* for the training process.[13] Figure 10 demonstrates the dynamicity and minimum value of the mean absolute error achieved by each of these models, as compared to *CVN-SFR*. According to this figure, it can be clearly seen that the minimum error has considerably increased in all cases. This observation justifies the necessity of using all the defined input parameters in the proposed model.[14]

[13] Each new model consists of 4 input neurons, 2 hidden layers with respectively 4 and 3 neurons, and \$1\$ output neuron. Furthermore, similar to *CVN-SFR*, these models use the squared error loss function, the gradient descent optimizer, and the learning rate equal to 0.01.

[14] It should be stressed here that A_5 is embedded to compensate sparse data in case of a low proportion of CVs.

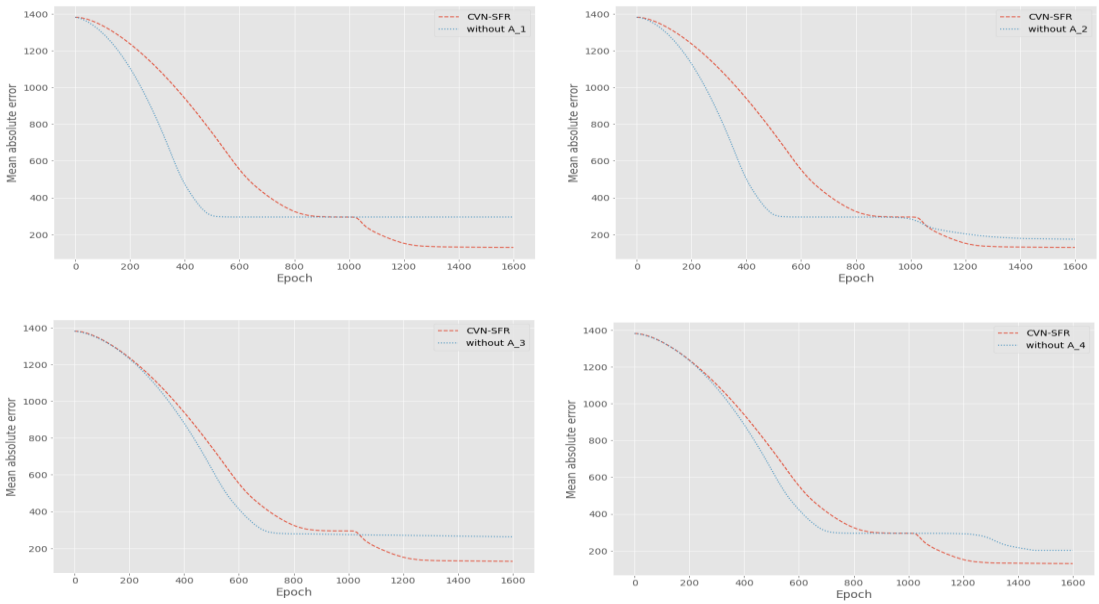

Figure 10. Investigating the effect of each input parameter on the minimum mean absolute error.

Future directions of CVN-SFR

As is shown in the previous section, we proposed an SFR estimation model that circumvents the limitations of conventional models by resulting in dynamic and accurate estimations of SFR through the use of information of CVs. This model as such is useful in that it can, eventually, lead to more efficient utilization of intersections capacity, especially at intersections with traffic-responsive control mechanisms whose specifications are connected to time-dependent conditions (including SFR). In this regard, by focusing on emerging CV-based intersection control mechanisms (due to the analogy of their input with *CVN-SFR* as the representative of traffic-responsive control mechanisms, it is expected to see future integration of related research endeavors.

It should however also be mentioned here that we have found *CVN-SFR* susceptible to errors when the communication zone (where vehicles send the related information of their approach to the corresponding intersection) is restricted due to reasons, such as (1) the limitations of the applied communication platform or (2) the limitations that might arise because of the intersection location against other traffic

network's settings.[15] In such a situation, the results of each input parameter in different temporal conditions are too close and, accordingly, the defined set of parameters would have a loose connection to the dynamics of SFR. In fact, to correctly include the effects of each input parameter, *CVN-SFR* needs a minimum communication zone (that is different for each intersection with respect to factors like the proportion of CVs in traffic), which in turn might limit the applicability of this model. Accordingly, the other important problem to be further studied can be: how to extend *CVN-SFR* in order to make it resilient to the above-mentioned limitation. One solution could be using more (but harder to get) pieces of CVs' data that can provide more robust results.

Conclusion

As it is expected that more and more CVs will share urban roads with conventional vehicles, the appropriate use of CVs information to manage traffic flows has become a matter of significant importance. However, while a considerable number of CV-based intersection control mechanisms have been proposed in the literature, the relation between the real-time information of CVs and the current SFR at each lane of an intersection has still remained an open area of active research. Inspired by this issue, we have presented a novel data-driven model (labeled by *CVN-SFR*) to leverage the information of CVs for enhancing the accuracy and dynamicity of SFR estimations.

To better explicate the implications of *CVN-SFR*, one should note that, apart from the dependence of SFR on the spatial constraints of an intersection, it is also sensitive to the time-varying parameters resulting from dynamicity and stochasticity inherent in traffic. Accordingly, the same intersection can have a different SFR with respect to

[15] For example, in dense networks where intersections are located very close to each other

parameters, such as the current traffic composition and the flow pattern. Concerning this point, the presented results in this paper have shown that *CVN-SFR* is capable of capturing such SFR dynamics

- to a large extent in the case of a high proportion of CVs;
- to some extent in the case of a low proportion of CVs.

Further simulations reported in this paper have confirmed that each of the defined input parameters is an important component of *CVN-SFR*. In this regard, the carried-out sensitivity analysis has shown that the functionality of the model can become far from being optimal in the case of eliminating each input parameter. On the other hand, concerning situations where the communication zone is restricted, there is still room for improvement of *CVN-SFR* by probably introducing new parameters using other pieces of CVs' data.

Acknowledgments

This work was partially supported by the Research Foundation Flanders (FWO) under Grant number 3G051118.

References

Abdi, Hervé, and Lynne J Williams. 2010. 'Principal Component Analysis', *Wiley Interdisciplinary Reviews: Computational Statistics*, 2: 433-59.

Adya, Monica, and Fred Collopy. 1998. 'How Effective Are Neural Networks at Forecasting and Prediction? A Review and Evaluation', *Journal of Forecasting*, 17: 481-95.

AG, PTV. 2018. *Vissim User Manual* (PTV Group: Germany).

Akçelik, Rahmi. 2008. "The Relationship between Capacity and Driver Behaviour." In *TRB National Roundabout Conference*.

Andayani, Ulfi, Ema Budhiarti Nababan, Baihaqi Siregar, Muhammad Anggia Muchtar, Tigor Hamonangan Nasution, and Ikhsan Siregar. 2017. "Optimization Backpropagation Algorithm Based on Nguyen-Widrom Adaptive Weight and Adaptive Learning Rate." In *2017 4th International Conference on Industrial Engineering and Applications (ICIEA)*, 363-67. IEEE.

Anusha, CS, Ashish Verma, and G Kavitha. 2013. 'Effects of Two-Wheelers on Saturation Flow at Signalized Intersections in Developing Countries', *Journal of Transportation Engineering*, 139: 448-57.

Arasan, Venkatachalam Thamizh, and Shriniwas Shrikant Arkatkar. 2008. "Estimating Passenger-Car Units for Vehicles of Heterogeneous Traffic Using Computer Simulation." In *Transportation Research Board 87th Annual Meeting*. Washington DC, United States.

Behbahani, Hamid, Mehdi Jahangir Samet, Vahid Najafi Moghaddam Gilani, and Amir Amini. 2017. "Determining of the Parking Manoeuvre and the Taxi Blockage Adjustment Factor for the Saturation Flow Rate at the Outlet Legs of Signalized Intersections: Case Study from Rasht City (Iran)." In *IOP conference series: materials science and engineering*, 042017. IOP Publishing.

Biswas, Sabyasachi, Souvik Chakraborty, Indrajit Ghosh, and Satish Chandra. 2018. 'Saturation Flow Model for Signalized Intersection under Mixed Traffic Condition', *Transportation Research Record*, 2672: 55-65.

Bonneson, James. 2005. "Guidelines for Quantifying the Influence of Area Type and Other Factors on Saturation Flow Rate." In.: Texas Transportation Institute, College Station, TX.

Brown, Marvin L, and John F Kros. 2003. 'Data Mining and the Impact of Missing Data', *Industrial Management and Data Systems*, 103: 611-21.

Brunton, Steven L, and J Nathan Kutz. 2022. *Data-Driven Science and Engineering: Machine Learning, Dynamical Systems, and Control* (Cambridge University Press).

Cai, Guang-Wei, Zhi Fang, and Yue-Feng Chen. 2019. "Estimating the Number of Hidden Nodes of the Single-Hidden-Layer Feedforward Neural Networks." In *2019 15th International Conference on Computational Intelligence and Security (CIS)*, 172-76. IEEE.

Chand, Subhash, Neelam Jain Gupta, and S Velmurugan. 2017. 'Development of Saturation Flow Model at Signalized Intersection for Heterogeneous Traffic', *Transportation Research Procedia*, 25: 1662-71.

Chen, Peng, Hideki Nakamura, and Miho Asano. 2012. 'Lane Utilization Analysis of Shared Left-Turn Lane Based on Saturation Flow Rate Modeling', *Procedia-Social and Behavioral Sciences*, 43: 178-91.

Chen, Peng, Hongsheng Qi, and Jian Sun. 2014. 'Investigation of Saturation Flow on Shared Right-Turn Lane at Signalized Intersections', *Transportation Research Record*, 2461: 66-75.

Flötteröd, Gunnar, and Jannis Rohde. 2011. 'Operational Macroscopic Modeling of Complex Urban Road Intersections', *Transportation Research Part B: Methodological*, 45: 903-22.

Gao, Jiti, Xiao Han, Guangming Pan, and Yanrong Yang. 2017. 'High Dimensional Correlation Matrices: The Central Limit Theorem and Its Applications', *Journal of the Royal Statistical Society: Series B*, 79: 677-93.

Gentile, Camillo, and Mario Sznaier. 2001. 'An Improved Voronoi-Diagram-Based Neural Net for Pattern Classification', *IEEE Transactions on Neural Networks*, 12: 1227-34.

Guo, Qiangqiang, Li Li, and Xuegang Jeff Ban. 2019. 'Urban Traffic Signal Control with Connected and Automated Vehicles: A Survey', *Transportation Research Part C: Emerging Technologies*, 101: 313-34.

Guo, Xiaoyu, Xiao Xiao, Yunlong Zhang, Chaolun Ma, and Shanglu He. 2019. "On Development of State-Based Fundamental Diagram for Signalized Intersection Using Connected

Vehicle Trajectory." In *Transportation Research Board 98th Annual Meeting*. Washington DC, United States.

Guo, Xiaoyu, and Yunlong Zhang. 2021. 'Estimating Fundamental Diagram for Signalized Intersections Using Connected Vehicle Data', *ITE Journal - Institute of Transportation Engineers*, 91: 42-48.

Guo, Yanming, Quan Yu, Yunlong Zhang, and Jian Rong. 2012. 'Effect of Bicycles on the Saturation Flow Rate of Turning Vehicles at Signalized Intersections', *Journal of Transportation Engineering*, 138: 21-30.

He, Qing, K Larry Head, and Jun Ding. 2014. 'Multi-Modal Traffic Signal Control with Priority, Signal Actuation and Coordination', *Transportation Research Part C: Emerging Technologies*, 46: 65-82.

Hecht-Nielsen, Robert. 1992. 'Theory of the Backpropagation Neural Network.' in, *Neural Networks for Perception* (Elsevier).

Hennink, Monique M. 2013. *Focus Group Discussions* (Oxford University Press).

Hossain, M. 2001. 'Estimation of Saturation Flow at Signalised Intersections of Developing Cities: A Micro-Simulation Modelling Approach', *Transportation Research Part A: Policy and Practice*, 35: 123-41.

Karlaftis, Matthew G, and Eleni I Vlahogianni. 2011. 'Statistical Methods Versus Neural Networks in Transportation Research: Differences, Similarities and Some Insights', *Transportation Research Part C: Emerging Technologies*, 19: 387-99.

Ke, Jinchuan, and Xinzhe Liu. 2008. "Empirical Analysis of Optimal Hidden Neurons in Neural Network Modeling for Stock Prediction." In *2008 IEEE Pacific-Asia Workshop on Computational Intelligence and Industrial Application*, 828-32. IEEE.

Kessels, Femke. 2019. 'The Fundamental Diagram.' in, *Traffic Flow Modelling* (Springer).

Lau, Mian Mian, and King Hann Lim. 2017. "Investigation of Activation Functions in Deep Belief Network." In *2017 2nd international conference on control and robotics engineering (ICCRE)*, 201-06. IEEE.

Lin, Feng-Bor. 1992. 'Saturation Flow and Capacity of Shared Permissive Left-Turn Lane', *Journal of Transportation Engineering*, 118: 611-30.

Little, Roderick JA, and Donald B Rubin. 2019. *Statistical Analysis with Missing Data* (John Wiley & Sons).

Michalopoulos, Panos G, and Gregory Stephanopoulos. 1981. 'An Application of Shock Wave Theory to Traffic Signal Control', *Transportation Research Part B: Methodological*, 15: 35-51.

Milazzo, Joseph S, Nagui M Rouphail, Joseph E Hummer, and D Patrick Allen. 1998. 'Effect of Pedestrians on Capacity of Signalized Intersections', *Transportation Research Record*, 1646: 37-46.

Moradi, Hossein, Sara Sasaninejad, Sabine Wittevrongel, and Joris Walraevens. 2021. 'Proposal of an Integrated Platoon-Based Round-Robin Algorithm with Priorities for Intersections with Mixed Traffic Flows', *IET Intelligent Transport Systems*, 15: 1106-18.

Moradi, Hossein, Sara Sasaninejad, Sabine Wittevrongel, and Joris Walraevens. 2022. 'The Contribution of Connected Vehicles to Network Traffic Control: A Hierarchical Approach', *Transportation Research Part C: Emerging Technologies*, 139: 103644.

Potts, Ingrid B, John F Ringert, Karin M Bauer, John D Zegeer, Douglas W Harwood, and David K Gilmore. 2007. 'Relationship of Lane Width to Saturation Flow Rate on Urban and Suburban Signalized Intersection Approaches', *Transportation Research Record*, 2027: 45-51.

Qin, Zhengtao, Jing Zhao, Shidong Liang, and Jiao Yao. 2019. 'Impact of Guideline Markings on Saturation Flow Rate at Signalized Intersections', *Journal of Advanced Transportation*, 2019: 1786373.

Radhakrishnan, Padmakumar, and Tom V Mathew. 2011. 'Passenger Car Units and Saturation Flow Models for Highly Heterogeneous Traffic at Urban Signalised Intersections', *Transportmetrica*, 7: 141-62.

Raj, Pooja, Kalaanidhi Sivagnanasundaram, Gowri Asaithambi, and Ravi Shankar. 2019. 'Review of Methods for Estimation of Passenger Car Unit Values of Vehicles', *Journal of Transportation Engineering, Part A: Systems*, 145: 04019019.

Saha, Arpita, Souvik Chakraborty, Satish Chandra, and Indrajit Ghosh. 2018. 'Kriging Based Saturation Flow Models for Traffic Conditions in Indian Cities', *Transportation Research Part A: Policy and Practice*, 118: 38-51.

Seo, Toru, Yutaka Kawasaki, Takahiko Kusakabe, and Yasuo Asakura. 2019. 'Fundamental Diagram Estimation by Using Trajectories of Probe Vehicles', *Transportation Research Part B: Methodological*, 122: 40-56.

Shao, Chang-qiao, and Xiao-ming Liu. 2012. 'Estimation of Saturation Flow Rates at Signalized Intersections', *Discrete Dynamics in Nature and Society*, 2012: 720474.

Shao, Chang-qiao, Jian Rong, Xiao-ming Liu, and Behavioral Sciences. 2011. 'Study on the Saturation Flow Rate and Its Influence Factors at Signalized Intersections in China', *Procedia-Social and Behavioral Sciences*, 16: 504-14.

Tan, Jiyuan, Li Li, Zhiheng Li, Yi Zhang, and Practice. 2013. 'Distribution Models for Start-up Lost Time and Effective Departure Flow Rate', *Transportation Research Part A: Policy*, 51: 1-11.

Thota, Lalitha Saroja, and Suresh Babu Changalasetty. 2013. 'Optimum Learning Rate for Classification Problem with Mlp in Data Mining', *International Journal of Advances in Engineering and Technology*, 6: 35.

TRB. 2010. *Hcm2010* (Transportation Research Board, National Research Council: Washington).

Uhlemann, Elisabeth. 2015. 'Introducing Connected Vehicles', *IEEE Vehicular Technology Magazine*, 10: 23-31.

Vasilyev, Vladimir. 2016. "Structural Design of Shallow Neural Networks on the Basis of Minimal Complexity Principle." In *2016 24th Mediterranean Conference on Control and Automation (MED)*, 1212-17. IEEE.

Wang, Linhong, Yunhao Wang, and Yiming Bie. 2018. 'Automatic Estimation Method for Intersection Saturation Flow Rate Based on Video Detector Data', *Journal of Advanced Transportation*, 2018.

Wang, Yi, Jian Rong, Chenjing Zhou, Xin Chang, and Siyang Liu. 2020. 'An Analysis of the Interactions between Adjustment Factors of Saturation Flow Rates at Signalized Intersections', *Sustainability*, 12: 665.

Wang, Yi, Jian Rong, Chenjing Zhou, and Yacong Gao. 2020. 'Dynamic Estimation of Saturation Flow Rate at Information-Rich Signalized Intersections', *Information*, 11: 178.

Yang, Dong-Yuan, Jiang-Lin Luo, Chong Liu, and Zheng-Yu Duan. 2013. 'Dynamic Extraction Method of Saturation Flow Rate at Signalized Intersection', *Jiaotong Yunshu Gongcheng Xuebao*, 13: 98-103.

Yang, Kaidi, Nan Zheng, and Monica Menendez. 2017. 'Multi-Scale Perimeter Control Approach in a Connected-Vehicle Environment', *Transportation Research Procedia*, 23: 101-20.